



The University of
Nottingham

UNITED KINGDOM · CHINA · MALAYSIA

Ershova, Olga V. and Klos, Jacek and Besley, Nicholas A. and Wright, Timothy G. (2015) Interaction of the NO $3p\pi$ ($C\ 2\Pi$) Rydberg state with RG (RG = Ne, Kr, and Xe): potential energy surfaces and spectroscopy. *Journal of Chemical Physics*, 142 (3). 034311/1-034311/15. ISSN 0021-9606

Access from the University of Nottingham repository:

<http://eprints.nottingham.ac.uk/28800/1/Published%20Article.pdf>

Copyright and reuse:

The Nottingham ePrints service makes this work by researchers of the University of Nottingham available open access under the following conditions.

- Copyright and all moral rights to the version of the paper presented here belong to the individual author(s) and/or other copyright owners.
- To the extent reasonable and practicable the material made available in Nottingham ePrints has been checked for eligibility before being made available.
- Copies of full items can be used for personal research or study, educational, or not-for-profit purposes without prior permission or charge provided that the authors, title and full bibliographic details are credited, a hyperlink and/or URL is given for the original metadata page and the content is not changed in any way.
- Quotations or similar reproductions must be sufficiently acknowledged.

Please see our full end user licence at:

http://eprints.nottingham.ac.uk/end_user_agreement.pdf

A note on versions:

The version presented here may differ from the published version or from the version of record. If you wish to cite this item you are advised to consult the publisher's version. Please see the repository url above for details on accessing the published version and note that access may require a subscription.

For more information, please contact eprints@nottingham.ac.uk

**Interaction of the NO 3p π (C 2 Π) Rydberg state with RG (RG = Ne, Kr, and Xe):
Potential energy surfaces and spectroscopy**

Olga V. Ershova, Jacek Kłos, Nicholas A. Besley, and Timothy G. Wright

Citation: *The Journal of Chemical Physics* **142**, 034311 (2015); doi: 10.1063/1.4905563

View online: <http://dx.doi.org/10.1063/1.4905563>

View Table of Contents: <http://scitation.aip.org/content/aip/journal/jcp/142/3?ver=pdfcov>

Published by the [AIP Publishing](#)

Articles you may be interested in

[Chirality of weakly bound complexes: The potential energy surfaces for the hydrogen-peroxide–noble-gas interactions](#)

J. Chem. Phys. **141**, 134309 (2014); 10.1063/1.4897136

[Interaction of the NO 3p \$\pi\$ Rydberg state with Ar: Potential energy surfaces and spectroscopy](#)

J. Chem. Phys. **138**, 214313 (2013); 10.1063/1.4808027

[Theoretical study of Al + – RG \(RG = He – Rn \)](#)

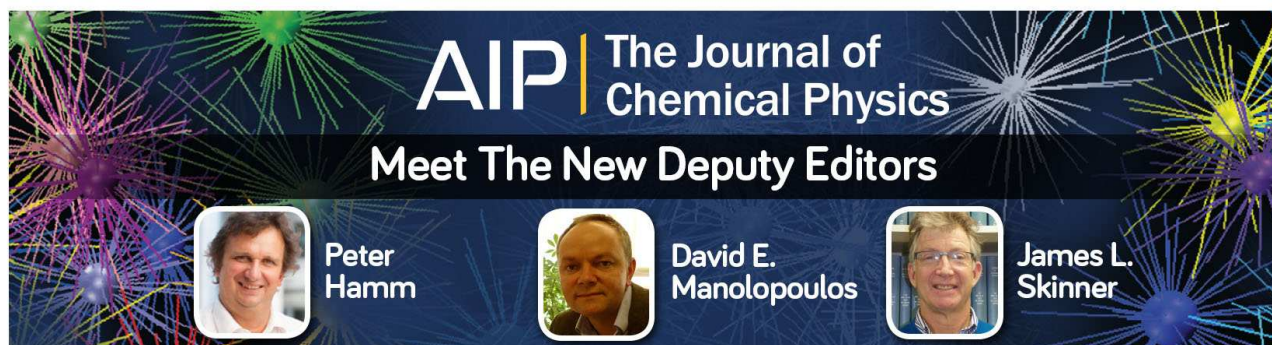
J. Chem. Phys. **133**, 164302 (2010); 10.1063/1.3494602

[Interaction of NO \(A \$\Sigma\$ 2 + \) with rare gas atoms: Potential energy surfaces and spectroscopy](#)

J. Chem. Phys. **129**, 244303 (2008); 10.1063/1.3040074


[Scattering of aligned molecules. The potential energy surfaces for the Kr-O 2 and Xe-O 2 systems](#)


J. Chem. Phys. **109**, 3898 (1998); 10.1063/1.476989




AIP | The Journal of
Chemical Physics

Meet The New Deputy Editors

 Peter Hamm

 David E. Manolopoulos

 James L. Skinner

Interaction of the NO $3p\pi$ ($C^2\Pi$) Rydberg state with RG (RG = Ne, Kr, and Xe): Potential energy surfaces and spectroscopy

Olga V. Ershova,¹ Jacek Klos,^{2,a)} Nicholas A. Besley,^{1,b)} and Timothy G. Wright^{1,c)}

¹*School of Chemistry, University of Nottingham, University Park, Nottingham NG7 2RD, United Kingdom*

²*Department of Chemistry and Biochemistry, University of Maryland, College Park, Maryland 20742-2021, USA*

(Received 13 November 2014; accepted 24 December 2014; published online 21 January 2015)

We present new potential energy surfaces for the interaction of NO($C^2\Pi$) with each of Ne, Kr, and Xe. The potential energy surfaces have been calculated using second order Møller-Plesset perturbation theory, exploiting a procedure to converge the reference Hartree-Fock wavefunction for the excited states: the maximum overlap method. The bound rovibrational states obtained from the surfaces are used to simulate the electronic spectra and their appearance is in good agreement with available (2+1) REMPI spectra. We discuss the assignment and appearance of these spectra, comparing to that of NO-Ar. © 2015 AIP Publishing LLC. [<http://dx.doi.org/10.1063/1.4905563>]

I. INTRODUCTION

In previous work,¹ we presented a new potential energy surface for the interaction of the nitric oxide molecule in its $3p\pi$ Rydberg state, NO($C^2\Pi$), with Ar, yielding the NO($C^2\Pi$)-Ar molecular complex. The surface was calculated using Møller-Plesset (MP2) theory, with the maximum overlap method (MOM)^{2,3} being used to help prevent variational collapse of the wavefunction. Note that at non-linear geometries, the $\tilde{C}^2\Pi$ state of the complex will split into $^2A'$ and $^2A''$ surfaces and these may variationally collapse to lower states, including those arising from the ground state, $\tilde{X}^2\Pi$ —hence our use of the MOM technique.

Interest in the NO molecule arises as it is a stable, open-shell molecule with a $^2\Pi$ ground state and interactions of open-shell molecules with closed-shell partners, particularly RG (RG = rare gas) atoms, are model systems for the investigation of so-called pre-reactive complexes, which can exhibit incipient chemical bonding.^{4,5} The apparent simplicity of the NO-RG systems does not do credit to the difficulty in interpreting the electronic spectra of these species, which arises from the complexity of the underlying rovibronic structure.

Recall that for NO, there are a set of Rydberg states that arise from the excitation of the $2p\pi^*$ electron into the $n\lambda$ Rydberg orbitals.⁶ It is expected that as n gets larger, then the properties of the Rydberg states⁷⁻⁹ will converge to those of the ground state cation, NO⁺. Things are somewhat more complicated in NO-RG complexes where there is competition for the cationic core between the Rydberg electron and the RG atom. In particular, for the lowest Rydberg state, the $3s\sigma$ state ($\tilde{A}^2\Sigma^+$), this leads to NO-Ar being more weakly bound than the \tilde{X} state, and hence, the electronic spectrum is blue-shifted compared to the corresponding spectrum in NO. This is attributed to the greater electron repulsion in the $\tilde{A}^2\Sigma^+$ state

compared to the $\tilde{X}^2\Pi$ state:¹⁰ essentially, the Ar atom is forced to be positioned outside of the Rydberg orbital and the \tilde{A} state may be viewed as Ar weakly interacting with NO($A^2\Sigma^+$). For NO-Ne, this also seems to be the case and actually leads to the NO-Ne \tilde{A} state not supporting any bound levels.¹¹ On the other hand, the \tilde{A} state of each of NO-Ar, NO-Kr, and NO-Xe all contain bound levels, but the spectra are not straightforward to assign, with most work having focused on NO-Ar,^{10,12-14} but with work on the NO-Kr and NO-Xe \tilde{A} states having been reported (see Ref. 15 and references therein). Previously, we have calculated the potential energy surfaces of the $\tilde{A}^2\Sigma^+$ Rydberg state of the NO-RG (RG = He-Xe) complexes using quantum chemical methods, and shown that the previous interpretations of the spectra for NO-Ar were incorrect, and at the same time, we provided insight into the assignment of the $\tilde{A} \leftarrow \tilde{X}$ spectra of NO-Kr and NO-Xe.¹⁶

As mentioned earlier, more recently we focused our attention on the NO($C^2\Pi$)-Ar complex,¹ obtaining very good agreement between the simulated $\tilde{C} \leftarrow \tilde{X}$ spectrum and that of the experiment. As we showed in that work, the reported \tilde{C} state spectrum of NO-Ar is almost exclusively carried by the A'' component, with the contribution from the A' component being small; this is mainly an effect of the Franck-Condon factors (FCFs).

In principle, at non-linear geometries, there are possible complications which can arise from interactions between the $\tilde{C}(A')$ component and the nearby $\tilde{D}^2\Sigma^+$ ($3p\sigma$) state, as the latter also becomes of A' symmetry. However, the dominance of the $\tilde{C}(A'')$ contribution to the spectrum and the very good agreement between the calculated and experimental spectrum in Ref. 1 indicates that these complications do not significantly affect the main \tilde{C} state spectrum. Here, we extend the work in our earlier \tilde{C} state paper on NO-Ar and report results for the \tilde{C} state of each of NO-RG (RG = Ne, Kr, and Xe); we do not explicitly consider interactions with the \tilde{D} state.

The $\tilde{C}^2\Pi$ ($v_{\text{NO}} = 0$) state spectra of NO-Ne and NO-Kr have been reported by Miller and Cheng,¹⁷ using resonance-enhanced multiphoton ionization (REMPI) spectroscopy. In

^{a)}Email: JKlos@umd.edu

^{b)}Email: Nick.Besley@nottingham.ac.uk

^{c)}Email: Tim.Wright@nottingham.ac.uk

addition, Miller¹⁸ published an improved spectrum for NO-Kr ($\nu_{\text{NO}} = 0$) and also a corresponding one for NO-Xe. Interestingly, while the spectra for NO-Ne and NO-Kr were recorded in the [NO-RG]⁺ mass channel, the spectra for NO-Xe were recorded in the Xe⁺ mass channel (recall that the initial electronic excitation is on NO); the latter aspect was discussed by Miller in that work, as well as others¹⁹—this will be further commented on below. Vastly improved \tilde{C} state REMPI spectra have been published for NO-Ne ($\nu_{\text{NO}} = 1, 2, \text{ and } 4$) by Fleniken *et al.*,²⁰ and for NO-Kr ($\nu_{\text{NO}} = 0$) by Mack *et al.*,²¹ with the latter paper also reporting the corresponding NO-Xe spectrum again, which was shown to be similar to that of Miller.²¹ Meyer and coworkers have suggested an interpretation of the \tilde{C} state spectra^{20,21} in terms of progressions of intermolecular stretches and bends, but with associated structure attributable to rotation of the complex about the *a* inertial axis (almost coincident with the Jacobi *R* direction) being a key aspect of the spectrum. This interpretation built on the model put forward by Meyer to explain the NO-Ar spectrum²²—see also Ref. 1.

II. COMPUTATIONAL DETAILS

A. Quantum chemistry calculations

All of the calculations have been performed using the Q-Chem quantum chemistry package.²³ Potential energy surfaces (PESs) for the ${}^2A''$ and ${}^2A'$ surfaces, arising from the \tilde{C} ${}^2\Pi$ Rydberg state of each of the NO-RG van der Waals complexes (RG = Ne, Kr, and Xe) have been calculated using MOM^{2,3} together with HF theory and second order MP2 perturbation theory to account for electron correlation energy (referred as MOM-MP2 in the following). In our previous work on NO-Ar,¹ it was demonstrated that the MOM-MP2 method yields results in good agreement with the MOM-CCSD(T) approach, but the former is clearly much less expensive, and so we exclusively use this approach here. MOM determines the excited state wavefunction directly within the self-consistent field calculation by preventing variational collapse to the ground state. It has been shown that MOM provides an accurate description of excited Rydberg states of NO when used in conjunction with density functional theory (DFT) or coupled cluster theory,²⁴ and this conclusion was supported by our previous work on the \tilde{C} state of NO-Ar.¹ However, when MOM-DFT was applied to the first Rydberg state, \tilde{A} ${}^2\Sigma^+$, of the NO-Ar complex,^{25,26} it was concluded that currently available DFT methods are not adequate for describing this system.

The unrestricted formalism of HF theory (UHF) has been used in all calculations, and the degree of spin contamination was small, with a maximum deviation from the exact value of 0.75 for $\langle S^2 \rangle$ of less than 0.01. For NO-Ne and NO-Kr, the doubly augmented, correlation-consistent d-aug-cc-pVQZ basis set^{27–30} was used in calculations of the PESs. To investigate the effect of basis set size for these, additional calculations were undertaken with d-aug-cc-pVTZ basis sets.

For NO-Xe, the larger number of electrons makes the calculations very computationally demanding and relativistic effects could start to become noticeable; for this reason, we switched to using an effective core potential (ECP), with

the ECP28MDF³¹ one being used for Xe. We were unable to use the full d-aug-cc-pVQZ-PP valence basis set for Xe with an ECP for technical reasons, and therefore, the non-ECP electrons of Xe were described by the d-aug-cc-pVTZ-PP basis set;³¹ for N and O, d-aug-cc-pVTZ basis sets were employed. Since we used a different basis set for Xe compared to the other species, we performed test calculations to assess their reliability. We did this by employing the ECP10MDF ECP for Kr, together with the d-aug-cc-pVTZ-PP basis set for the non-ECP electrons and comparing these results to the all-electron calculations.

The NO bond length is fixed at 1.062 Å in our NO-RG calculations, which is its equilibrium gas-phase value, r_e , in the $C^2\Pi$ state.³² This is justified owing to the high frequency of the NO stretch compared to the intermolecular vibrations; in previous work on NO⁺-Ar, the effect of the NO⁺ stretch on the calculated intermolecular surface was found to be negligible,³³ and similar behaviour is expected for the higher-lying Rydberg states.

Counterpoise-corrected PESs for the interaction of NO with each RG were constructed in the Jacobi coordinates *R* and θ , where *R* is the distance between the NO centre of mass and RG, and θ is the angle between the NO molecular axis and the line connecting the RG nucleus with the NO centre of mass; $\theta = 0^\circ$ corresponds to the RG-N-O linear geometry and $\theta = 180^\circ$ to the RG-O-N geometry. The *ab initio* calculations have been done on grids of *R* and θ with the following values:

For NO-Ne (${}^2A''$): *R* = 5.0-12.0 bohrs in steps of 0.5 bohr, plus 5.75 and 6.25 bohrs; $\theta = 0^\circ$ - 180° in steps of 20° plus 90° .

For NO-Ne (${}^2A'$): *R* = 5.0-12.0 bohrs in steps of 0.5 bohr, plus 5.75 and 6.25 bohrs; $\theta = 0^\circ$ - 180° in steps of 20° .

For NO-Kr (${}^2A''$): *R* = 5.5-12.0 bohrs in steps of 0.5 bohr, plus 6.25 and 6.75 bohrs; $\theta = 0^\circ$ - 180° in steps of 10° .

For NO-Kr (${}^2A'$): *R* = 5.5-12.0 bohrs in steps of 0.5 bohr, plus 6.25 and 6.75 bohrs; $\theta = 0^\circ$ - 180° in steps of 10° excluding 90° , where there were convergence problems.

For NO-Xe (${}^2A''$): *R* = 6.0-12.0 bohrs in steps of 0.5 bohr, plus 6.25, 6.75, and 7.25 bohrs; $\theta = 0^\circ$ - 180° in steps of 10° .

For NO-Xe (${}^2A'$): *R* = 6.0-12.0 bohrs in steps of 0.5 bohr, plus 6.25, 6.75, and 7.25 bohrs; $\theta = 0^\circ$ - 180° in steps of 10° , excluding 80° and 90° , where there were convergence problems.

When constructing the surfaces using the MOM approach, it was found to be important to carry out the excitation at long *R* values, where the identity of the orbitals is clear, and then to scan to shorter *R*, ensuring that each surface was continuous. At the shorter *R* values, there is mixing of the $3p\sigma$ and $3p\pi$ *a'* orbitals into each of the $\tilde{C}(A')$ and \tilde{D} state wavefunctions, and so, some caution was required to ensure the correct energy was being associated with the correct state. Only the $\tilde{C}(A')$ surface is considered here, the \tilde{D} state will be considered in future work.

B. Bound rovibrational state calculations

In order to simulate the $\tilde{C} \leftarrow \tilde{X}$ spectrum, we need a wavefunction for the initial state of the NO($X^2\Pi$)-RG

complex from which the transition originates. This initial state is characterized by a total angular momentum quantum number $J = 1/2$, corresponding to a state with a non-rotating NO molecule ($r = 0$ in terms of pure rotational quantum number, $n = 1$ in terms of total angular momentum minus spin). The ground state wavefunction, which we will denote $|\tilde{X}, J = 1/2\rangle$ is obtained from Coupled States (CS)³⁴ calculations that account for the open-shell nature of the NO(X) molecule and were performed with the Hibridon program.³⁵ We used the most recent A' and A'' NO(X)-RG potentials produced by Kłos *et al.* for RG = Ne,³⁶ Kr,³⁷ and Xe.³⁸ The rovibrational calculations are performed using the V_{sum} and V_{diff} potentials as described by Alexander.³⁹ To converge the bound states of the $J = 1/2$ NO(X)-RG complex, we used a rotational basis for the NO molecule with j running up to 10.5 with a rotational constant $B_0 = 1.69611 \text{ cm}^{-1}$ and spin-orbit constant $A_{\text{SO}} = 123.1393 \text{ cm}^{-1}$ for the NO(X) molecule.^{32,40} The pseudo-diatomic reduced masses for each of the NO-RG complexes employed were 11.9970, 22.0980, and 24.4398 amu for RG = Ne, Kr, and Xe, respectively. (Note that this implies we only considered the isotopologue with the most prevalent isotope for all atoms, in particular, ²⁰Ne, ⁸²Kr, and ¹³¹Xe.) With this set of parameters and choice of potential, the energy of the ground $J = 1/2$ state is calculated to be at -35.03 , -111.95 , and -116.95 cm^{-1} with respect to the corresponding RG + NO(X $^2\Pi$) asymptote, for RG = Ne, Kr, and Xe, respectively. For the two heavier species, these are in extremely good agreement with the experimental D_0'' values¹⁵ of 105.4 and 121.3 cm^{-1} for NO-Kr and NO-Xe, respectively; excellent agreement is also seen with the previous⁴¹ NO-Ne calculated value of 35 cm^{-1} . The wavefunction for the ground state is represented on a discrete numerical grid by an evenly distributed set of 52 Gaussian functions⁴² along R between 4.5 and 25 a_0 , and a set of rotational basis wavefunctions of the NO molecule expressed by Wigner rotation functions of given j and ω values.⁴³

The electronically excited state of a NO molecule with $3p\pi$ Rydberg character is denoted $C^2\Pi$ and lies at $T_e = 52\,126 \text{ cm}^{-1}$ above the ground $X^2\Pi$ ground state.³² As for the \tilde{X} state, the resulting NO(C)-RG complex will similarly be characterized by adiabatic potential energy surfaces belonging to A' or A'' irreducible representations of the C_s symmetry group. To calculate the bound states of each NO($C^2\Pi$)-RG complex, we used spin-including open-shell CS calculations in Hibridon similar to those described above in case of the \tilde{X} state in conjunction with the $\tilde{C}(A')$ and $\tilde{C}(A'')$ PESs computed in the present work (see below); the calculations were again performed using the V_{sum} and V_{diff} potentials.³⁹ The following spectroscopic parameters of the NO($C^2\Pi$) molecule were used:⁴⁴ $B_0 = 1.99377 \text{ cm}^{-1}$, $A_{\text{SO}} = 3.2 \text{ cm}^{-1}$, $p = -1.2 \times 10^{-2}$, and $q = -1.6 \times 10^{-2} \text{ cm}^{-1}$. To converge all of the bound states with $J = 0.5 - 2.5$, we used a rotational basis for NO($C^2\Pi$) up to $j = 18.5$, with 131 Gaussians along the radial R coordinate from 4.0 to 30.0 a_0 . All wavefunctions are represented on a discrete numerical grid in a similar fashion as for the ground state wavefunction. We will denote the excited state wave functions by $|\tilde{C}, J, P, v\rangle$, where v labels the vibrations.

To simulate each NO-RG $\tilde{C} \leftarrow \tilde{X}$ spectrum, we assume that the transition originates from the ground $|\tilde{X}, J = 1/2\rangle$ state with NO in its ground vibrational state. To calculate the Franck-Condon factors needed for spectral line intensities, we use rovibronic wavefunctions of the NO($C^2\Pi$)-RG complex calculated for $J = 1/2, 3/2$, and $5/2$. We also assume that the electronic transition dipole moment of NO is constant. The spectral line intensities are calculated as in our previous work¹⁶ as a squared sum of integrals of products of ground and excited state wave functions with $P_{1,m}(\cos \Theta)$ ($m = -1, 0, 1$) Legendre functions representing the components of the parallel ($m = 0$) and perpendicular ($m = \pm 1$) transition dipole moment, d

$$I(J; J', P', v') \propto |\langle \tilde{X}, J'' = 0.5 | d | \tilde{C}, J', P', v' \rangle|^2, \quad (1)$$

where $''$ refers to the initial state and $'$ to the final state, J is the total angular momentum, P is the final projection quantum number, and v denotes a cumulative index for the vibrational quantum numbers.

Since the experimental spectrum is obtained in a two-photon process, then $\Delta J \leq 2$, allowing J values of $1/2, 3/2$, and $5/2$ to be accessed in the \tilde{C} state, from the lowest $J = 1/2$ level in the \tilde{X} state. The calculated energy levels are identified by their overall J number, as well as the projection of J on the a inertial axis, P . The total angular momentum arises from the electronic spin and orbital angular momentum, plus the rotational angular momentum. For the present system, the rotation of NO occurs in two directions: rotation in-plane, which becomes an intermolecular bend in the complex; and rotation out of plane, around the a inertial axis. With the a axis being almost coincident with the intermolecular axis, we see that rotation about this axis is close to being solely NO rotation, and so we expect to be able to see the structure associated with this in the spectrum; this was considered in detail by Meyer.²² We can represent this motion by a quantum number K_a . On the other hand, the (almost equivalent) rotation of the whole complex about either of the b and c axes each has a very large moment of inertia, owing to the movement of the RG atom about the centre of mass. As such, this structure was not resolved in the experimental spectra referred to in the present work, although it is considered in the simulation and calculation of the energy levels. This motion is represented by the quantum number L ; but, since these rotations produce rotational angular momentum perpendicular to the plane of the NO-RG complex, they do not affect the value of P . If it is assumed that the spin, S , becomes quantized along the a inertial axis of the complex, then it will have projections, $P_s = \pm 0.5$ —see Ref. 45 for more details.

III. RESULTS AND DISCUSSION

A. \tilde{C} state dissociation energies

In Table I, we show the D_e values calculated from the NO(\tilde{C}^2A'')-RG PES for NO-Ne, NO-Ar, and NO-Kr using different basis sets. For NO-Ar, single-point calculations at the MOM-MP2/d-aug-cc-pVTZ minimum energy geometry are performed employing d-aug-cc-pVXZ basis sets

TABLE I. Calculated (MOM-MP2) dissociation energies for the ${}^2A''$ component of the $\text{NO}(\tilde{C}^2\Pi)$ -RG complexes.

Basis set	D_e/cm^{-1a}			
	NO-Ne	NO-Ar	NO-Kr	NO-Xe
d-aug-cc-pVDZ	...	298.4
d-aug-cc-pVTZ	117.1	411.8	562.1	...
d-aug-cc-pVTZ-PP ^b	...		567.4	841.9
d-aug-cc-pVQZ	121.8	452.1	612.9	...
d-aug-cc-pV5Z	...	462.7
d-aug-cc-pV ∞ Z (D,T) ^c	...	459.5
d-aug-cc-pV ∞ Z (T,Q) ^c	125.2	481.6	649.8	...
d-aug-cc-pV ∞ Z (Q,5) ^c	...	473.7

^aThese have been calculated at the respective minima on the PES, except for the NO-Ar values, which are single-point energies calculated at the MOM-MP2/d-aug-cc-pVTZ optimized geometry ($R = 6.31 a_0$ and $\theta = 67.8^\circ$).

^bThis valence basis set was employed with an ECP: ECP10MDF (for Kr) and ECP28MDF (for Xe).

^cValues obtained from extrapolation to the basis set limit—see text.

($X = \text{D-5}$), with proximate pairs being used to obtain basis set extrapolated values for D_e , using the cubic formula. As is often the case, (D,T) extrapolation is not sufficient, usually because the double- ζ energy is poor, but both (T,Q) and (Q,5) extrapolations yield very similar values, suggesting these extrapolated values are reliable and give a best value of D_e (NO-Ar) = 475-480 cm^{-1} . For NO-Ne and NO-Kr, values for minimum energy geometries are presented for $X = \text{T}$ and Q and extrapolated. The (T,Q) extrapolation for NO-Ne yields 125 cm^{-1} with that for NO-Kr giving 650 cm^{-1} . As noted, only a single value was calculated for NO-Xe, for technical reasons, employing the ECP28MDF effective core potential with the d-aug-cc-pVTZ-PP valence basis set.

The A' and A'' PESs calculated with the MOM-MP2/d-aug-cc-pVQZ method are used for the simulations of the spectra for NO-Ne and NO-Kr; for NO-Xe, the MOM-MP2/(ECP28MDF+d-aug-cc-pVTZ-PP) method was employed. Thus, we expect the PESs to be more reliable for the two lighter species than for NO-Xe. From the spin-including calculations, the D_0 value could be obtained and for the NO-RG (\tilde{C}) states, these values were 85.2 cm^{-1} , 542.7 cm^{-1} , and 757.0 cm^{-1} for RG = Ne, Kr, and Xe, respectively.

We note that

$$D_0'' + T_0^{\text{NO}} = D_0' + T_0, \quad (2)$$

where D_0'' is the dissociation energy of the \tilde{X} state, D_0' is the dissociation energy of the \tilde{C} state, T_0 is the 0-0 vibronic transition of the complex, and T_0^{NO} is the 0-0 transition in bare NO. It can be seen from Table II that there is reasonable agreement between the experimental and calculated D_0' values, although, as Eq. (2) shows, each value is reliant on both the D_0'' value and the observation of the origin in the $\tilde{C} \leftarrow \tilde{X}$ spectrum—we shall come back to this point later.

B. Potential energy surfaces

The energies for the MOM-MP2/d-aug-cc-pVQZ A'' and A' , NO-Ne and NO-Kr PESs, and the ECP-based MOM-

MP2/d-aug-cc-pVTZ-PP PES for NO-Xe are given as supplementary material.⁴⁶ Contour plots of these PESs are shown in Figure 1, together with that of NO-Ar from our previous work,¹ for ease of comparison. The parameters associated with the equilibrium geometries and dissociation energies are given in Table II. In all cases, the lowest-lying PES corresponds to the A'' component of the \tilde{C} state, which can be associated with a negative value of the phenomenological quenching parameter, ϵ , used in Ref. 45. The ${}^2A''$ PES has a single minimum with an equilibrium geometry that is bent, with the RG atom closer to the N atom than the O. In line with expectations, R_e increases monotonically with the atomic number of the RG atom; in addition, the equilibrium Jacobi bond angle decreases as the atomic number of the RG atom increases, possibly attributable to an increase in the dipole-induced dipole interaction, as a result of the increasing polarizability of the RG atom, although clearly other factors are also contributing. The ${}^2A'$ PES for NO-Ne and NO-Kr, in contrast, both have linear minimum energy geometries, one at each end of the NO molecule; both are of very similar depths, with that at the N end of the molecule being the deeper. Interestingly, for NO-Xe, the global minimum on the ${}^2A'$ surface is not linear, but has a bent Xe-NO geometry, as for the ${}^2A''$ PES; there is, however, a minimum at the NO-Xe linear geometry. In all cases, the two components become degenerate at the linear geometries of the complex, forming the linear, doubly degenerate $\text{ON}(\tilde{C}^2\Pi)$ -RG (0°), and $\text{NO}(\tilde{C}^2\Pi)$ -RG (180°) species.

In Table II, we have included the optimized geometries and binding energies, D_e , for the cations from Ref. 47. The $\tilde{C}(A'')$ minimum energy geometry is expected to be quite similar to the relevant cation,⁴⁷ since the unpaired a'' electron is located out of plane and so the RG atom is able to interact with the partially exposed NO^+ core. As can be seen, this is indeed the case, with both equilibrium bond lengths and bond angles being quite similar. There is, however, a consistent observation that the cation's bond length is 0.2-0.4 Å shorter than the one for the corresponding $\tilde{C}({}^2A'')$ state, and this is in line with the significant differences in dissociation energy. This is expected, owing to repulsion between the RG electrons and the unpaired diffuse Rydberg electron. As for the cation, this skewed T-shaped geometry for the $\tilde{C}(A'')$ state is also consistent with the picture of the RG atom donating a small amount of electron density into the lowest unoccupied orbital—the $2p\pi^*$ orbital of NO.

The $\tilde{C}(A')$ PES lies above the $\tilde{C}(A'')$ PES, is shallower, and becomes degenerate at the corresponding linear regions of the $\tilde{C}(A'')$ surface. Additionally, at $\sim \theta = 90^\circ$, it may be seen that for the $\tilde{C}(A')$ PES, as the RG atom approaches from long R , there is a rise in energy as the dense region of the $3p\pi$ orbital is encountered. Again, this is expected, as the unpaired a' electron lies in-plane, perpendicular to the N-O axis, leading to significant electron repulsion between the Rydberg electron and the RG electrons when the geometry is close to being T-shaped. Indeed, in several cases, we encountered problems obtaining convergence in the UHF wavefunction at $\sim 90^\circ$, possibly as a result of the near-degeneracy of the $\tilde{C}({}^2A')$ and \tilde{D} state surfaces here.

TABLE II. Geometric parameters (Jacobi coordinates) at minima and dissociation energies for NO-RG(\tilde{X}) and NO-RG(\tilde{C}) complexes (RG = Ne–Xe).^a

Surface	R_e/a_0	$\theta_e/^\circ$	D_e/cm^{-1}	D_0/cm^{-1}	$D_0^{\text{spin}}/\text{cm}^{-1\text{b}}$	Experimental ^c
NO-Ne						
$\tilde{X}[^2\Pi(A'')]$	6.19	82.6	57.6	37.9	35.0	
$\tilde{X}[^2\Pi(A')]$	6.18	96.1	59.5	32.4		
$\tilde{C}[^2\Pi(A'')]$	5.78	72.7	121.8	85.7	85.2	113
$\tilde{C}[^2\Pi-(A')]$	7.11	0.0	72.6	12.8	[87.6]	
$\tilde{C}[^2\Pi-(A'')]$	6.81	180.0	60.3			
$\tilde{X}^+1\Sigma^+$	5.40	79.4	344.7			
NO-Ar						
$\tilde{X}[^2\Pi(A'')]$	6.90	71.9	115.0	89.6	86.7	94
$\tilde{X}[^2\Pi(A')]$	6.75	94.9	120.3	85.8		
$\tilde{C}[^2\Pi(A'')]$	6.24	67.6	449.8	387.3	386.2	412
$\tilde{C}[^2\Pi-(A')]$	7.58	0.0	246.8	152.3	[411.1]	
$\tilde{C}[^2\Pi-(A'')]$	7.58	180.0	238.3			
$\tilde{X}^+1\Sigma^+$	6.00	65.9	954			
NO-Kr						
$\tilde{X}[^2\Pi(A'')]$	7.21	66.0	143.1	115.6	112.0	105.4
$\tilde{X}[^2\Pi(A')]$	7.00	92.9	146.6	112.1		
$\tilde{C}[^2\Pi(A'')]$	6.45	65.0	612.8	543.0	542.7	567
$\tilde{C}[^2\Pi-(A')]$	7.80	0.0	324.0	279.4	[575.4]	
$\tilde{C}[^2\Pi-(A'')]$	7.50	180.0	323.5			
$\tilde{X}^+1\Sigma^+$	6.23	62.0	1300			
NO-Xe						
$\tilde{X}[^2\Pi(A'')]$	7.68	64.4	148.2	121.8	117.0	121.3
$\tilde{X}[^2\Pi(A')]$	7.46	93.6	148.7	116.4		
$\tilde{C}[^2\Pi(A'')]$	6.74	62.0	841.9	757.5	757.0	823
$\tilde{C}[^2\Pi-(A')]$	7.20	44.3	465.9	396.8		
$\tilde{C}[^2\Pi-(A'')]$	7.86	180.0	425.8			
$\tilde{X}^+1\Sigma^+$	6.39	58.5	1976			

^aThe \tilde{X} state values have been calculated from the surfaces described in the text.

^bThese values come directly from the spin-including calculations employing the surfaces described in the present work. The values in square brackets for the $^2A''$ state have been adjusted from these by the ratio of the quadruple- ζ and (T,Q) D_e values in Table I.

^cSee text for further details and discussion of the experimental results.

It is interesting to note from Table II that, close to the A'' state minimum, the A' and A'' surfaces are much closer together for the \tilde{X} state than they are for the \tilde{C} state. We attribute this to the stronger interaction in the \tilde{C} state, which leads to the RG atom being closer to the NO^+ core, and so also undergoing stronger interaction with the Rydberg-like $3p\pi$ electron; indeed, these are competing for the same region of space. This may be seen in molecular orbital plots (not shown) where for NO-Ar, it is clearly seen that the Ar atom is impinging on the $3p$ Rydberg orbital and this leads to electron repulsion. It is therefore unsurprising that there is a significantly weaker binding energy with the in-plane $3p\pi$ electron density, compared to the out-of-plane case where there is a nodal plane coincident with the molecular plane, leading to much stronger interaction of the RG with the partially exposed core. For the \tilde{X} state, the RG atom is largely outside of the main electron density, and significantly further away: hence, the two surfaces are much closer together. Additionally, increases in polarizability and dipole moment for the $C^2\Pi$ state of NO compared to the $X^2\Pi$ state will

be providing some contributions to the larger \tilde{C} state binding energy in the NO-RG complexes.

C. Simulated spectrum and assignment

As described above, and similar to our previous work,^{1,16} we have calculated bound rovibrational energy levels using both spin-free and spin-including calculations, with the Hibridon program, but we concentrate on the more-correct spin-including calculations here.³⁵ Note that in all cases, as was the case also for NO-Ar,¹ the calculated D_0 value for the $\tilde{C}(A'')$ component of the NO-RG from the spinless calculation is very close to the spin-included value (see Table II) suggesting that the influence of the A' surface on the spectroscopy will be small. (In Ref. 1, we showed that the simulated spectrum arising from the $^2A''$ surface was very close to that of the full spin-including calculation.) For NO-RG (RG = Ne, Kr, and Xe, respectively), the spin-including calculations yield a range of bound states that are supported

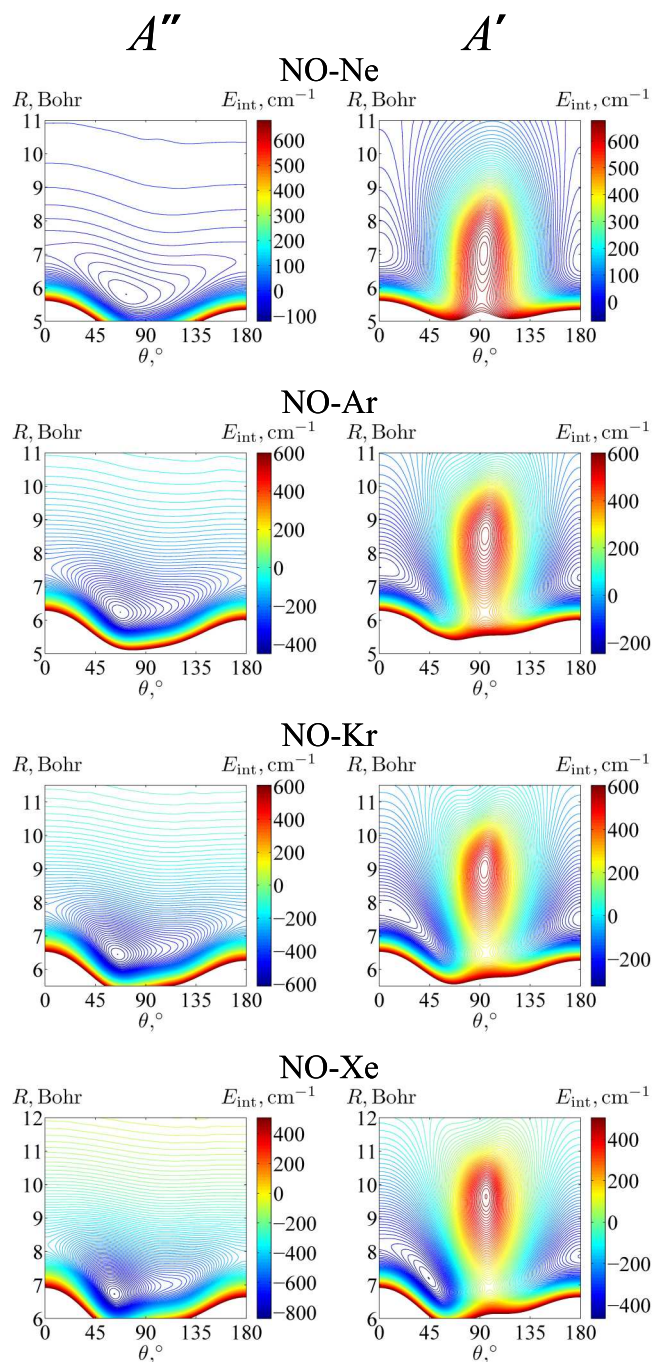


FIG. 1. Contour plots of the A'' and A' potential energy surfaces calculated in the present work: the level of theory employed for the \tilde{C} state was MOM-MP2 and each point was counterpoise corrected—see text for further details.

by the potential energy surface for $(J = 1/2, P)$, $(J = 3/2, P)$, and $(J = 5/2, P)$, where P is the projection quantum number of the total angular momentum, J . Full tables of the calculated bound states are available as supplementary material.⁴⁶ These energy levels, together with the associated wavefunctions, have been used to simulate the $\tilde{C} \leftarrow \tilde{X}$ spectrum. Each line in the simulated spectrum is made up of a number of transitions, corresponding to different (J, P, L) combinations; however, since the spectra to which we compare do not resolve the end-over-end motion, we do not refer to the L quantum number in our analysis below, but note that each line in the present

simulated spectrum is actually made up of a number of transitions corresponding to different L contributions. Since the complex is a reasonably strongly bound, skewed T-shaped complex, the levels may also be looked at in terms of intermolecular vibrational progressions with associated K_a structure, as noted above. The intermolecular bending modes and the K_a motion (rotation of NO about the a principal axis) have their origins in the rotational energy levels of the free NO motion, which evolves as a result of the interaction with the RG atom, described by correlation diagrams whose form depends on the magnitude of the various intermolecular potential matrix elements, V_{JL} .⁴⁸ What the correlation diagrams in Ref. 48 show is that for large, negative V_{20} values, corresponding to linear species, the NO bending levels are those for the degenerate bending mode; while for large, positive V_{20} values (T-shaped species), the levels split into non-degenerate bending levels and levels from rotation of NO (essentially equivalent to rotation of the complex) about the a inertial axis, the K_a levels. The latter is essentially the present case, where the molecule is a slightly skewed T-shape. In addition, there is interaction with the spin, which becomes quantized along the a axis, leading to (unresolved) spin-rotation splitting of the K_a levels.⁴⁵ The lowest $J = 0.5, P = 0.5$ level evolves from the $v = 0$ bending vibration of the linear complex, and will be the $K_a = 0$ level of the zero-point vibrational level in the T-shaped complex. The next level can be thought of as evolving from one of the components of the degenerate linear bend from the RG-NO ${}^2\Pi_{1/2}$ state, with $P = 0.5$ but there is also $P = 1.5$ character arising from the vibrationless level of the RG-NO ${}^2\Pi_{3/2}$ state (see discussion in Ref. 1 for NO-Ar). In the “T-shaped” complex, these can both be thought of as $K_a = 1$ levels, but split by spin-rotation into the different P levels. In a similar way, the next two features arise from $K_a = 2$ and $K_a = 3$ levels, with the first having two contributions ($P = 1.5$ and 2.5), while the second only has $P = 2.5$, as we have restricted the value of J to ≤ 2.5 . We expect this series of K_a lines to be associated with each vibration, although the intensities and spacings can change as a result of vibrationally averaged geometry changes and changing interaction in different regions of the PES.

With the above discussion in mind, to assign each spectrum we first look for all contributing bands that correspond to $J = 0.5$ and $P = 0.5$. Such bands arise in pairs, corresponding to the pure vibrational band ($K_a = 0$) and also, a few cm^{-1} higher, a band corresponding to the same vibration and $K_a = 1$. By looking at the contours of the nuclear wavefunction in the (R, θ) plane of the lowest-energy feature, it was usually possible to identify the nature of the vibration as a stretch, a bend, a combination band, or a progression member of one of these. Thus, we assign the transitions in terms of their contributing vibrational level in terms of the intermolecular stretch quantum number, v_σ and the intermolecular bend quantum number, v_β . As noted, each of these will have the associated $K_a = 0, 1, 2,$ and 3 levels. As will be seen, the bend and stretch motions become coupled to differing extents and at different energies up the potential well for the different species, so sometimes the assigned quantum numbers will be approximate.

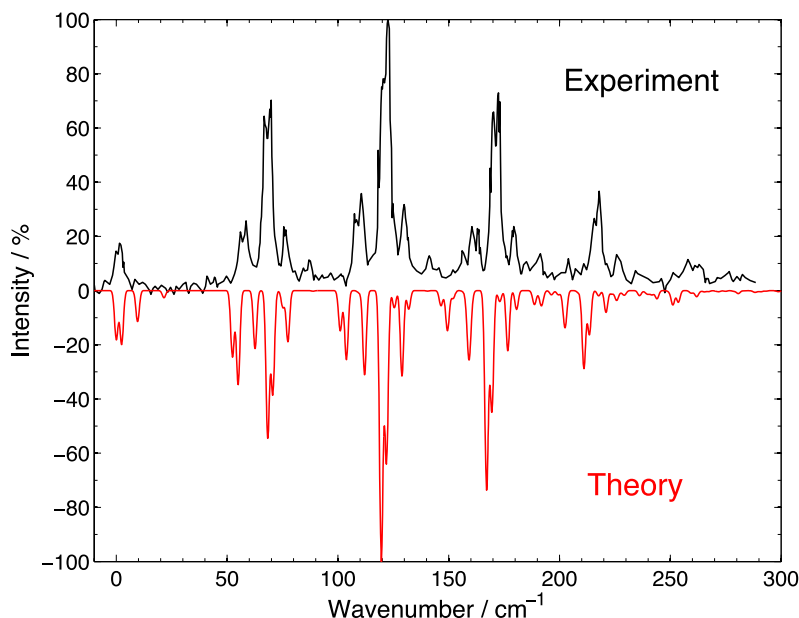


FIG. 2. Upper trace: experimental (2+1) REMPI spectrum of the $\tilde{C}^2\Pi \leftarrow \tilde{X}^2\Pi$ transition of NO-Kr, with the trace digitized from Ref. 21. Lower trace: simulation of the $\tilde{C}^2\Pi \leftarrow \tilde{X}^2\Pi$ spectrum of NO-Kr employing spin-including calculations. See text for details.

We commence by discussing the spectrum of NO-Kr, as it is the most similar to the previous example of NO-Ar.¹

1. NO-Kr

Our best, spin-including, calculated spectrum of the $\tilde{C} \leftarrow \tilde{X}$ transition, $v_{\text{NO}} = 0$, for NO-Kr is shown as an inverted trace in Figure 2. The simulated NO-Kr spectrum is obtained from the set of calculated Franck-Condon factors using a Gaussian convolution with a FWHM of 1.8 cm^{-1} . The experimental spectrum, digitized from Ref. 21, is shown as the upright trace. The agreement may be seen to be in excellent qualitative and, for the most part, even quantitative agreement with the experimental spectrum, similar to our previous results for NO-Ar.¹ In Figure 3, we show the simulated spectrum again, but also indicate the positions of the $J = 0.5$, $P = 0.5$ lines. As noted, these appear in pairs, one for $K_a = 0$ and one for $K_a = 1$; we show the contour of the vibrational wavefunction for the lower one, which corresponds to the pure (rotationless) vibration.

The first main feature appears in the experimental spectrum between 0 and 25 cm^{-1} . It consists of three lines and is very well reproduced by the simulation, with the latter showing that there is actually a very weak fourth line to higher wavenumber. These four lines are the K_a levels, as in NO-Ar,¹ and are all associated with the zero-point vibrational level. This may be seen in Figure 3, where the vibrational wavefunction of this lowest line is clearly the zero-point vibrational level. In our previous paper¹ on NO-Ar, we showed that the “vibrational” wavefunctions function for the two P contributions to the $K_a = 1$ level were different: for $P = 1.5$, the wavefunction corresponded to a zero-point-energy function, while for $P = 0.5$, the wavefunction resembled a bending vibration. These can be viewed as contributions from the $v = 0$ and $v = 1$ bending levels of the linear complex each from the different spin-orbit levels, now manifested as spin-rotation splitting of the $K_a = 1$ level; similar behavior is observed for the $K_a = 2$

level, while for the $K_a = 3$ level, only one spin-rotation level is included in the simulation because of the condition $J \leq 2.5$.

To slightly higher energy, $45\text{--}95 \text{ cm}^{-1}$, is a second group of lines, which the experimental spectrum appears to show consists of 4 main components (see Figure 2), although the simulation suggests there are more, but they are overlapping. The lowest energy line has $J = 0.5$, $P = 0.5$ only and so corresponds to a rotationless vibration (see Figure 3); its vibrational wavefunction indicates it is largely an intermolecular stretch ($\nu_{\sigma} = 1$), but also has significant bending character, seen from the fact that the node is not horizontal. Associated with this, we expect the same pattern of K_a features as on the origin with similar relative intensities, which does seem to be the case, although these start to overlap the next set of K_a levels; this commences at the most intense line in this feature, which also has $J = 0.5$, $P = 0.5$. The vibrational wavefunction (see Figure 3) of this line indicates that this band is largely an intermolecular bend ($\nu_{\beta} = 1$), but also has significant stretching character, indicated by the non-vertical direction of the node (see Figure 3). Associated with this band are the four different K_a levels, as expected, but the fourth one is very weak. It is interesting that the form of the vibrational wavefunctions indicates significant bend/stretch mixing even at these low energies. It is also interesting that the vibration that is predominantly a bend appears to higher energy than the vibration that is predominantly a stretch. Finally, we note that the appearance of the $45\text{--}95 \text{ cm}^{-1}$ region is slightly different from the experimental spectrum, and perhaps suggests that the intermolecular stretch is calculated to be slightly low, so that the associated $K_a = 3$ band should actually be closer to the intense intermolecular bend $K_a = 0$ feature, and so appear as a shoulder; and indeed, this feature does appear to be broad—see Figure 2.

The next main feature is in the range $100\text{--}140 \text{ cm}^{-1}$, and has even more lines (see Figure 2), which can be attributed to overlapping K_a levels from three vibrations: the overtones of the bend and stretch, as well as the bend-stretch combination

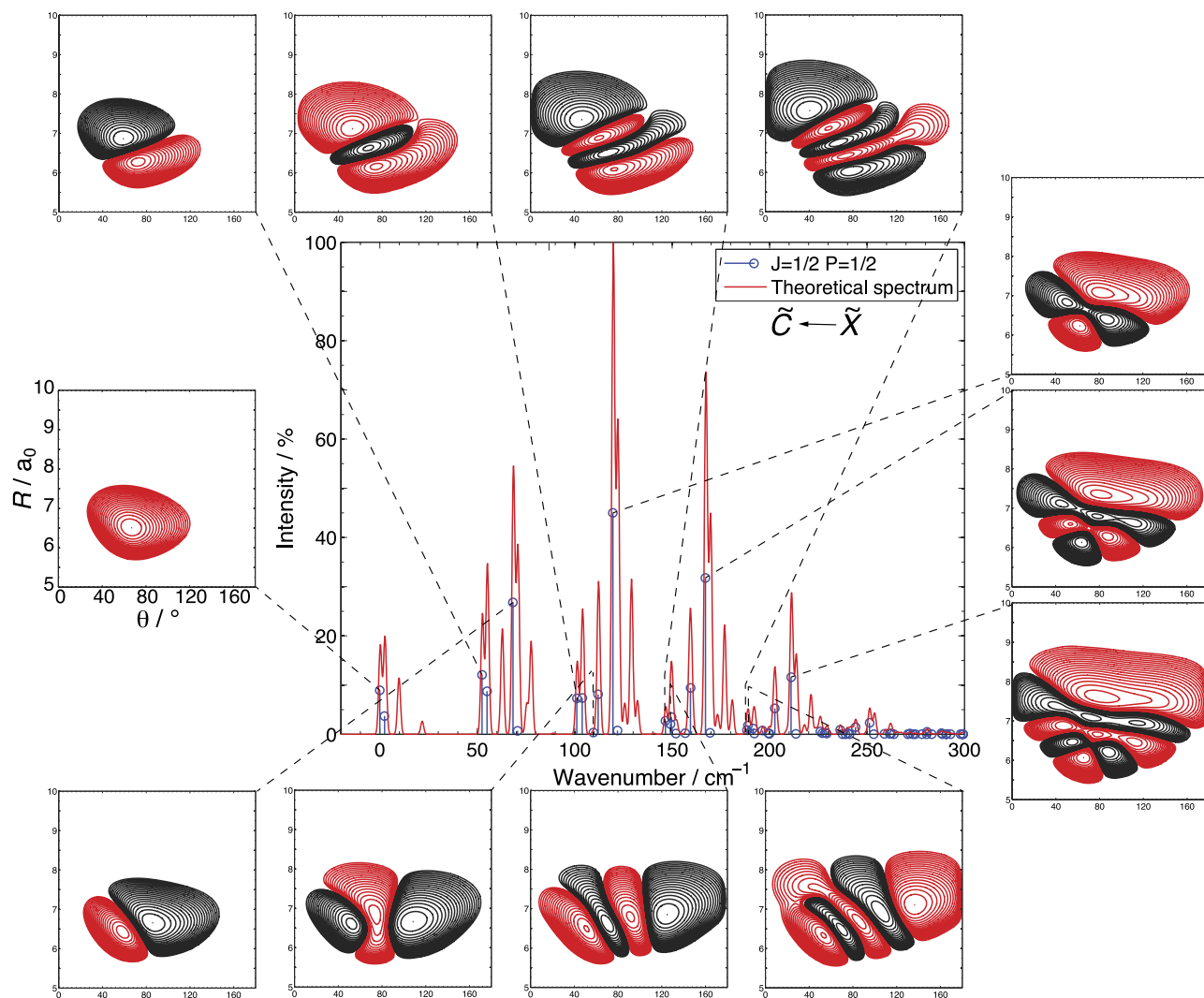


FIG. 3. Simulation of the $\tilde{C}^2\Pi \leftarrow \tilde{X}^2\Pi$ spectrum of NO-Kr employing spin-including calculations. The vertical lines mark the positions of $J = 0.5$, $P = 0.5$ lines: for each pair of these, the lower corresponds to the rotationless ($K_a = 0$) line, while the other gives a contribution to the $K_a = 1$ line. For the main (rotationless) stretch progression (top row) and bend progressions (bottom row), we give calculated vibrational contours, as well as for selected combination bands (right vertical column). The axes are the same for all of the contour plots: note that the zero-point vibrational wavefunction plot (centre, left-hand side) shows the axes labels in a larger font.

($v_\sigma = 1$, $v_\beta = 1$). The $K_a = 0$ levels associated with each of these features can be picked out straightforwardly from the “stick” form of the spectrum (Figure 3), but these overlap heavily in the convoluted spectrum. It is apparent that when looking at the vibrational wavefunctions, with the caveat that these are somewhat mixed, the first line (and associated K_a levels) should be associated with the overtone of the stretch, the next set of K_a levels are associated with the bend, and the most intense feature appears to be associated with the stretch-bend combination band. That said, it is evident from the wavefunctions that there is some mixing between the stretch overtone and the stretch-bend combination and hence some ambiguity as to which is which. We opt for the series of wavefunctions at the top of Figure 3 being a stretch progression, and those down the right-hand side as being combination bands based upon the similarity of the former to the $v_\sigma = 1$ wavefunction, and the appearance of the central region of the latter, which suggests both bend and stretch contributions. This assignment gives rise to the peculiarity

that the combination band is above the overtones of both contributing vibrations, but we emphasise the mixed nature of these modes (which are likely in Fermi resonance).

The next feature is a set of lines appearing in the range 140–190 cm^{-1} . In this region, we expect to see bands associated with the following: ν_β^3 , ν_σ^3 , $\nu_\beta^2\nu_\sigma$, and $\nu_\beta\nu_\sigma^2$. Based on the form of the (rotationless) vibrational wavefunctions, some of which are quite mixed, our best assignment for these features gives the ordering of these vibrations as ν_σ^3 , ν_β^3 , $\nu_\beta^2\nu_\sigma$, and $\nu_\beta\nu_\sigma^2$, each having associated K_a levels, with the most intense feature corresponding to $\nu_\beta\nu_\sigma^2$.

In the range 190–230 cm^{-1} , features arising from five different vibrations are expected: ν_β^4 , ν_σ^4 , $\nu_\beta^3\nu_\sigma$, $\nu_\beta^2\nu_\sigma^2$, and $\nu_\beta\nu_\sigma^3$. Our best assignment gives the ordering as ν_σ^4 , ν_β^4 , $\nu_\beta^3\nu_\sigma$, $\nu_\beta^2\nu_\sigma^2$, and $\nu_\beta\nu_\sigma^3$, with the most intense feature corresponding to $\nu_\beta\nu_\sigma^3$; again, we emphasise that a number of these vibrations are substantially mixed.

We note that krypton has a number of naturally occurring isotopes, although the predominant one is ^{82}Kr . The per-

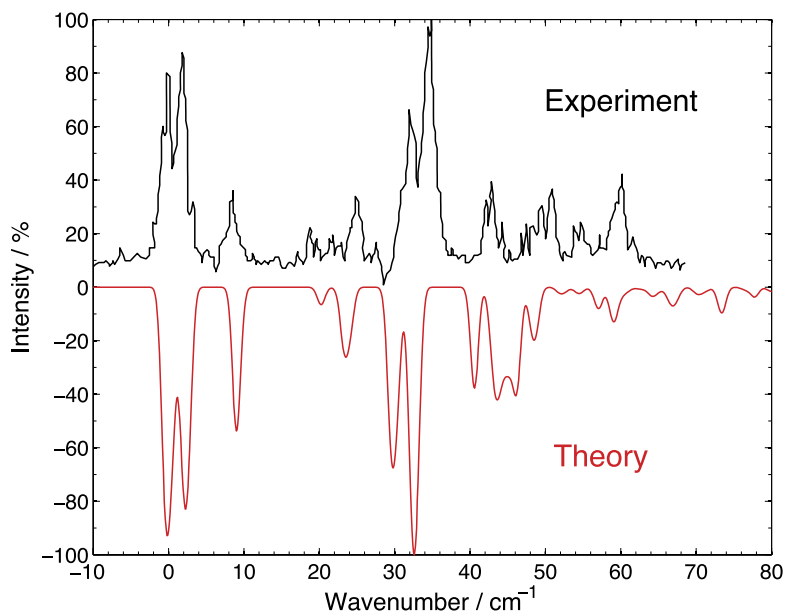


FIG. 4. Upper trace: experimental (2+1) REMPI spectrum of the $\tilde{C}^2\Pi \leftarrow \tilde{X}^2\Pi$ transition of NO-Ne ($\nu_{\text{NO}} = 1$) with trace digitized from Ref. 20. Lower trace: simulation of the $\tilde{C}^2\Pi \leftarrow \tilde{X}^2\Pi$ spectrum of NO-Ne employing spin-including calculations. See text for details.

centage change in the spectroscopic parameters from the other isotopologues is expected to be small, and indeed, in Ref. 21, it was noted that whether all isotopologues or a single one of $[\text{NO-Kr}]^+$ was gated in the recording of the REMPI spectrum, the appearance of the spectrum was not affected to any noticeable extent within the resolution. The present simulations are for the most prevalent isotopologue, NO- ^{82}Kr .

In Ref. 21, a simulation of the $\tilde{C} \leftarrow \tilde{X}$ spectrum of NO-Kr was presented in which, for each vibration, the K_a spacings were adjusted to best-fit the experiment, by varying the Jacobi angle of the Kr atom and adjusting the relative intensity of the overall vibration band, but with the relative intensities of the contributing K_a levels (each vibration gives rise to four K_a features) obtained from projection of the two-photon dipole moment operator onto the a inertial axis. We note that no combination bands were considered in Ref. 21, with the spectrum being assigned to progressions of the pure intermolecular bend and stretch vibrations. The present work generally concurs with this latter assignment, except in two aspects. First, our results suggest that combination bands are important, but there is much overlapping of features; and second, the bend and stretch motions become significantly mixed. In addition, there can also be Fermi-resonance mixing between energetically proximate vibrations as well.

Also of note is that for a number of the vibrations, the pattern of four K_a peaks with a similar intensity and spacing pattern can be discerned, in agreement with the implications of the simulation in Ref. 21. However, further up in wavenumber, the present simulation suggests that this is not the case, and perturbations occur, particularly for the intensities. That the overall simulation is so good suggests that the assignments suggested by our simulation are largely correct, and that the agreement of the empirically fitted simulation of Ref. 21 must be due to the fitting process, which is compensating for, for example, the non-inclusion of combinations. On the whole, given the fact that the present calculation is obtained directly from quantum

chemical calculations, the agreement with experiment and the fitted simulation from Ref. 21 is very satisfying.

2. NO-Ne

Our best simulated spectrum for NO-Ne is shown in Figure 4 as an inverted trace, with the experimental trace being the upright one and corresponding to the $\nu_{\text{NO}} = 1$ $\tilde{C} \leftarrow \tilde{X}$ REMPI spectrum, with the trace digitized from Ref. 20. The simulated NO-Ne spectrum is obtained from the set of calculated Franck-Condon factors using a Gaussian convolution with a FWHM of 1.2 cm^{-1} . In the absence of interactions between different electronic states, we do not expect the intermolecular surface to be affected to any significant extent by the different vibrational excitation of the NO moiety. The first set of features between 0 and 10 cm^{-1} is very similar to that in NO-Kr, and can be assigned to the $K_a = 0, 1,$ and 2 levels of the zero-point level; the simulation suggests that the $K_a = 3$ line appears higher up in wavenumber, close to 20 cm^{-1} , and is contributing to the first weak feature of the next set of lines.

Searching for $J = 0.5, P = 0.5$ lines, we see that these again appear in pairs, with the lower corresponding to the rotationless, vibrational transition. The weak band at $\sim 20 \text{ cm}^{-1}$ in the simulation has a contribution from a $J = 0.5, P = 0.5$ line, with the vibrational wavefunction (see Figure 5) being clearly a bend; it is notable that the relative intensity of the $K_a = 0$ and $K_a = 1$ levels of the bend are different from those of the zero-point level. The intense set of lines forming the feature between 30 and 40 cm^{-1} can be seen from Figure 5 to arise from the intermolecular stretch, with the first feature being $K_a = 0$, and the more intense feature being $K_a = 1$. We then have a series of weaker features in the experimental spectrum to higher wavenumber, which are not so well reproduced by the simulation. The main part of the simulated feature is made up of three combinations: two forming the more intense part at $\sim 40\text{-}50 \text{ cm}^{-1}$ and some weaker features just past this; however, the lowest wavenumber line is actually the $K_a = 2$ line associated with

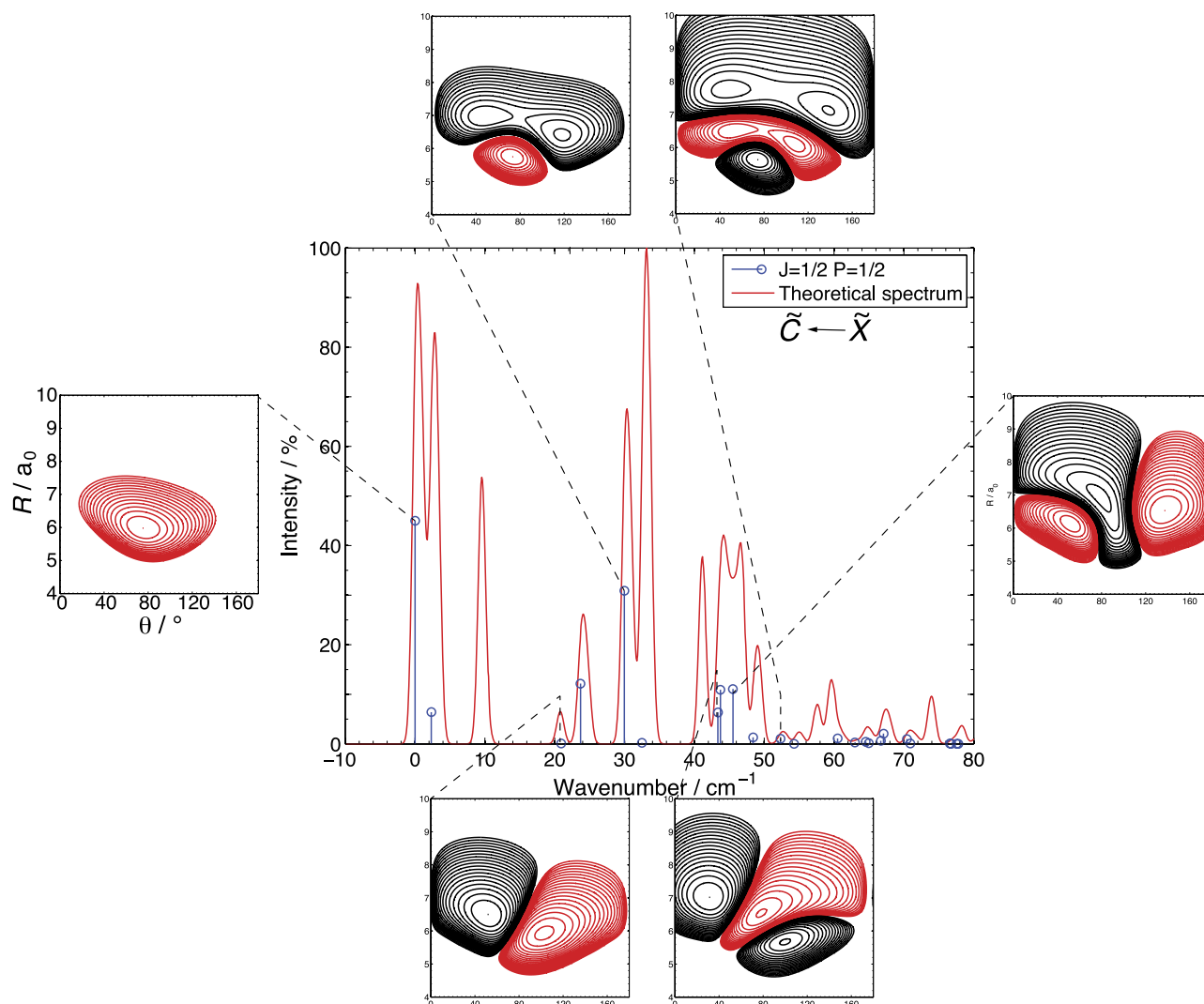


FIG. 5. Simulation of the $\tilde{C} \ ^2\Pi \leftarrow \tilde{X} \ ^2\Pi$ spectrum of NO-Ne employing spin-including calculations. The vertical lines mark the positions of $J = 0.5$, $P = 0.5$ lines: for each pair of these, the lower corresponds to the rotationless ($K_a = 0$) line, while the other gives a contribution to the $K_a = 1$ line. For the main (rotationless) stretch progression (top row) and bend progressions (bottom row), we give calculated vibrational contours, as well as for a selected combination band (right vertical column). The axes are the same for all of the contour plots: note that the zero-point vibrational wavefunction plot (centre, left-hand side) shows the axes labels in a larger font.

the intermolecular stretch. Other features are expected to be, and can be identified as, the overtones of the bend and the stretch as well as the bend-stretch combination band, from the vibrational wavefunction contour plots presented in Figure 5. The latter suggest that the energy ordering is that the overtone of the bend appears first, with the bend-stretch combination band very close in energy, then, the overtone of the stretch is weaker and to higher wavenumber. In all cases, there is evidence of bend-stretch mixing as the nodes are not all completely horizontal or vertical, but, perhaps surprisingly for this weakly-bound system, the vibrations are reasonably described as bends, stretches, or combinations thereof.

The weaker bonding of NO-Ne makes it more prone to having hot bands populated. We investigated this and it seemed that some of the experimental features to the red of the main bands could be attributable to hot features; however, it was not possible to be conclusive on this as the match in intensities was not overwhelmingly convincing. The experimental REMPI spectrum was mass-resolved and

is of the NO- ^{20}Ne isotopologue—it was found that the spectrum of the isotopologue NO- ^{22}Ne was identical within the experimental resolution.²⁰ We also note that in Ref. 20, well-resolved spectra were recorded for $\nu_{\text{NO}} = 2$ and, to a lesser extent, $\nu_{\text{NO}} = 4$ although the spectra were broadening as ν_{NO} increased. In Ref. 17, the spectrum corresponding to $\nu_{\text{NO}} = 0$ was reported, but the resolution was not as good as that in Ref. 20, and so the structure is not so clear. Subtle differences in the appearance of the spectra for different ν_{NO} was attributed to interactions between the \tilde{C} and \tilde{B} states.

Fleniken *et al.* also reported a simulation of the $\tilde{C} \leftarrow \tilde{X}$ spectra, with their procedure having been outlined in the above for NO-Kr, and we note that there are small differences between the spectra recorded for different ν_{NO} values, which they attributed to interactions between vibrational levels in the \tilde{C} and \tilde{B} states. Given that the structure associated with each vibrational component of the simulated spectrum was adjusted (by varying geometric parameters) to fit the experiment, the agreement with the present simulation (Figure 4)

is quite remarkable. We note, however, that combination bands were apparently not considered in the simulation in Ref. 20. In addition, the appearance of our simulation and the experiment suggests that the “simple” K_a pattern of four peaks for each vibration is changing significantly with intermolecular vibrational level (both the position and the intensity), and so the high wavenumber region of the simulation in Ref. 20 (which is not in as good agreement with experiment, similar to the present work) may not be so reliable. Part of this may be in relation to the transition dipole moment, which is assumed to be constant across the band; in the present work, it may also be due to the potential energy surface not being sufficiently accurate in the weakly bound region of the potential.

In summary, the overall simulation in the present work, which contains no fitting to experimental data, suggests the main aspects of the spectroscopy are correct, but that further improvements in the already high-level surface may be required for even better agreement. This is particularly true of the high wavenumber region and perhaps suggests that the region of the surface close to dissociation is not as reliable as the lower part. Additionally, a better understanding of how hot features could be affecting the appearance of the experimental spectrum would be useful.

3. NO-Xe

In Figure 6, we show our best simulated spectrum of NO-Xe together with the experimental spectrum. The simulated NO-Xe spectrum is obtained from the set of calculated Franck-Condon factors using Gaussian convolution with FWHM of 3.5 cm^{-1} . The overall profile of the spectrum is correct, but it is clear that the structure is only in qualitative agreement. We note that the weak nature of the lowest few bands is replicated, as is the sizeable gap to the next feature. Thereafter, there appear to be pairs of bands in the experimental spectrum, which are not immediately apparent in the simulation, but this will be discussed further below.

Looking at the simulated spectrum and picking out the bands corresponding to $J = 0.5$, $P = 0.5$, see Figure 7, it is clear that these pairs of features each consists of two features: one feature that is composed of the very close $K_a = 0$ and $K_a = 1$ lines; while the second is associated with the $K_a = 2$ line. The $K_a = 3$ line is weaker and appears to higher energy. Looking at the pattern of lines, it appears that if the A rotational constant, which depends on the vibrationally averaged Jacobi angle, was smaller, then the $K_a = 0, 1$ and the $K_a = 2$ lines would be closer together, and this would lead to closer agreement with the apparent pairs of lines in the experimental spectrum. Given that the NO-Xe PES was calculated with a smaller basis set, it is possible that our optimized geometry could be improved to give better agreement with the observed spectrum. Notwithstanding this, the general appearance of the spectrum suggests that our assignment should be reasonable, and we outline this next—further discussion on this is presented below.

First, we note that because NO-Xe is more strongly bound than the other species, the bend and stretch motions are not as mixed as for the other species; hence, for much of the observed spectrum, it is straightforward to pick out the different rotationless ($J = 0.5$, $P = 0.5$) vibrational bands and assign stretch and bend quantum numbers to them—Figure 7. Rather unusually, we find that the intermolecular stretch corresponds to the first main rotationless feature at $\sim 60\text{ cm}^{-1}$ in the simulation, with the next rotationless feature (at $\sim 90\text{ cm}^{-1}$) being the intermolecular bend. It is then possible to follow progressions of these vibrations up the spectrum, noting that various combination bands appear in between these. Figure 7 illustrates the main bend and stretch progressions, as well as selected combinations.

In trying to understand the poorer agreement in the case of NO-Xe, in contrast to the much better agreement for NO-Ar and NO-Kr and, to a slightly lesser extent, NO-Ne, we considered a number of issues. First, recall that this surface was calculated employing a smaller valence basis set, and additionally employed an ECP. The use of an ECP

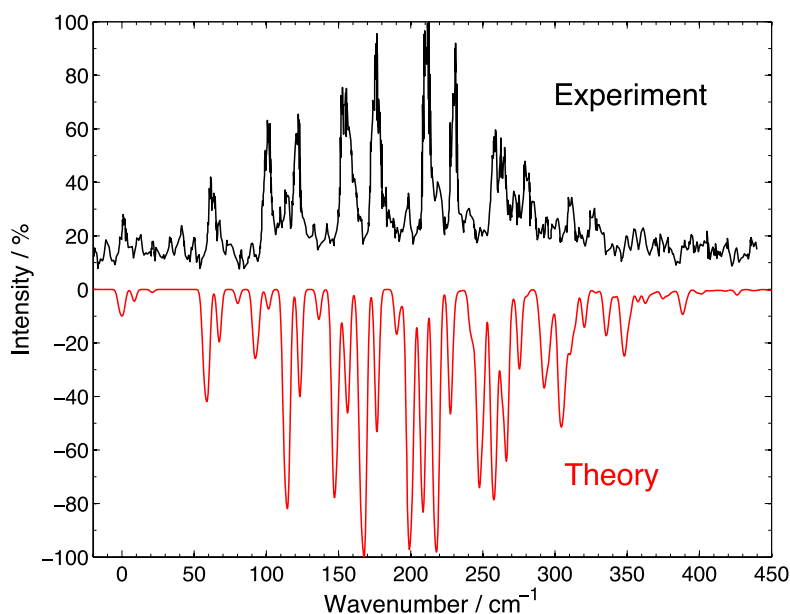


FIG. 6. Upper trace: experimental (2+1) REMPI spectrum of the $\tilde{C}^2\Pi \leftarrow \tilde{X}^2\Pi$ transition of NO-Xe, with the trace digitized from Ref. 21. Lower trace: simulation of the $\tilde{C}^2\Pi \leftarrow \tilde{X}^2\Pi$ spectrum of NO-Xe employing spin-including calculations. See text for details.

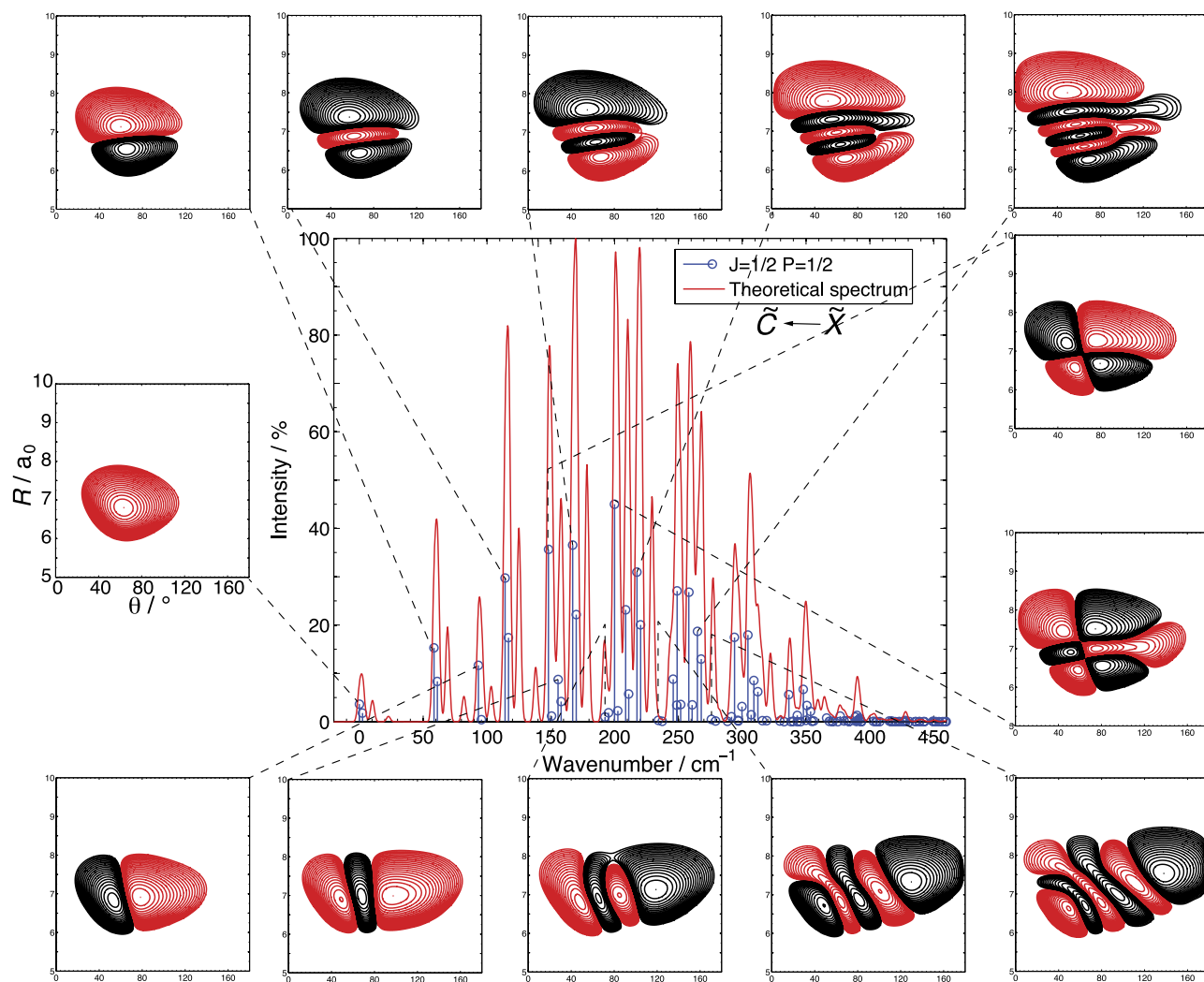


FIG. 7. Simulation of the $\tilde{C} \ ^2\Pi \leftarrow \tilde{X} \ ^2\Pi$ spectrum of NO-Xe employing spin-including calculations. The vertical lines mark the positions of $J = 0.5$, $P = 0.5$ lines: for each pair of these, the lower corresponds to the rotationless ($K_a = 0$) line, while the other gives a contribution to the $K_a = 1$ line. For the main (rotationless) stretch progression (top row) and bend progressions (bottom row), we give calculated vibrational contours, as well as for selected combination bands (right vertical column). The axes are the same for all of the contour plots: note that the zero-point vibrational wavefunction plot (centre, left-hand side) shows the axes labels in a larger font.

does not seem to be an issue, as the calculated dissociation energies for NO-Kr employing all-electron and ECP-based basis sets led to very similar results (see above and Table I). On the other hand, the smaller basis set does lead to a lower calculated dissociation energy (Table I), and therefore is expected to lead to calculated vibrational energy levels that are probably slightly low and slightly too close in energy. This would certainly have an effect on the appearance of the spectrum, particularly the relative spacings of the stretch and bend progressions, and the mixing between these vibrations; but as noted, the overall appearance of the spectrum is reasonable. A second possible complication is the various naturally occurring Xe isotopes, since there are several isotopes with significant natural abundances; however, the percentage change in the key spectroscopic parameters is small and is not expected to lead to significant changes in the overall appearance of the spectrum.²¹ We also do not see any obvious evidence that hot band features are a cause of the problem. As noted above, the value of the A rotational constant (in part determined by the equilibrium Jacobi angle)

could be an issue, and could lead to a closing up of the K_a structure, and it is plausible that this could be having a significant effect, in particular, it could lead to the present simulated spectrum apparently showing more features owing to lines being predicted to be further apart, and so more complicated than the actual spectrum. It would be interesting at this point, to compare with simulations using the method of Meyer *et al.*; however, for NO-Xe, no satisfactory simulation of the spectrum was possible.²¹

There is one other key aspect of the $\tilde{C} \leftarrow \tilde{X}$ transition in NO-Xe that should be considered as possibly affecting the appearance of the spectrum, which we now examine. As noted above, the excitation in these complexes is localized on the NO molecule and is a $3p\pi \leftarrow 2p\pi^*$ excitation. Thus, when ionization occurs during the REMPI process, the positive charge is expected to be localized on NO^+ . It is possible that there will be fragmentation of the $\text{NO}^+\text{-Xe}$, but owing to the very large photoionization cross-section for NO, there will be a large number of NO^+ ions around in a REMPI experiment, and so such fragmentation products would be

hard to see definitively. However, the reported spectrum for the $\tilde{C} \leftarrow \tilde{X}$ transition in NO-Xe actually has been recorded in the Xe^+ mass channel and no NO^+ -Xe parent ions were observed. This is in stark contrast to the same transition in the three lighter complexes that were all recorded in the parent mass channel. (Note that for the $\tilde{A} \leftarrow \tilde{X}$ transition, the spectrum for NO-Ar was recorded in the parent mass channel only, while for NO-Kr and NO-Xe, the spectra were recorded in both the parent and RG^+ mass channels.¹⁵) The mechanism for production of the Xe^+ is not well understood, but has been discussed previously,^{18,19} and is thought to involve superexcited neutral states and resonant energy (charge) transfer between the RG and NO moieties. Such processes may well have an effect on the appearance of the spectrum and indeed, as noted in Ref. 21, attempts to simulate the spectrum met with no success and it was suggested that this may be due to such issues. It is clear, however, that the first step in the production of the spectrum is the $\tilde{C} \leftarrow \tilde{X}$ transition located on the NO molecule, which is the likely reason why the overall intensity profile looks in reasonable agreement with experiment, being determined by the Franck-Condon window for this transition. If such a mechanism was operating, it might initially be expected that the resulting spectrum would contain more features than the simple $\tilde{C} \leftarrow \tilde{X}$ spectrum; however, it may be that the involvement of the superexcited state leads to selective enhancement of features or even to higher-intensity new features, giving rise to an apparently simpler spectrum. We conclude that both further experimental and theoretical work is required for this complex. For example, recording two-colour REMPI spectra would allow control over the accessing of the superexcited states. It may perhaps also be concluded that the very good agreement for the NO-Ar, NO-Kr, and (mostly) NO-Ne suggests that the poorer agreement for NO-Xe indicates the severe demands on the quantum chemistry calculations.

D. Dissociation energies

In Table II, we show the calculated dissociation energies, D_0 , employing both spin-including calculations and those obtained from the separate $^2A''$ and $^2A'$ surfaces. As noted above, the values from the spin-including calculations are very close to those from the $^2A''$ surface and confirm the minor role played by the $^2A'$ surface on the observed spectroscopy here. To compare to the experimental \tilde{C} state D_0 values, we calculated these employing Eq. (2) and present the values in Table II. We take the transition energies for uncomplexed NO from Table II of Ref. 20, which are derived from data presented in Ref. 49. For NO-Ne, we employ the $\nu_{\text{NO}} = 1$ value from Ref. 20 for the origin of the \tilde{C} ($\nu_{\text{NO}} = 1$) $\leftarrow \tilde{X}$ transition and employ the calculated D_0 value for the \tilde{X} state of NO-Ne³⁶—this yields a D_0 value for \tilde{C} (NO-Ne) of 113 cm^{-1} , in fair agreement with our best calculated value of 87.6 cm^{-1} (Table II) For NO-Ar, again, we used the $\nu_{\text{NO}} = 1$ values using the NO transition energy from Ref. 20 and that of NO-Ar from Ref. 22. For the D_0 value for the \tilde{X} state, we take a value of 94 cm^{-1} , which is between the two most recent determinations of $93.8 \pm 0.9 \text{ cm}^{-1}$ (Ref. 50)

and $95.4 \pm 1.4 \text{ cm}^{-1}$ (Ref. 51). These values yield a D_0 value for \tilde{C} (NO-Ar) of 412 cm^{-1} , in excellent agreement with our best calculated value 411.1 cm^{-1} (Table II). For NO-Kr, we take the $\nu_{\text{NO}} = 0$ value for the transition energy of NO from Ref. 20, with the value for NO-Kr being taken from Ref. 21; the \tilde{X} state D_0 value is taken as 105.4 cm^{-1} from Ref. 15. These values yield a D_0 value for \tilde{C} (NO-Kr) of 567 cm^{-1} , which is in very good agreement with our best value of 575.4 cm^{-1} . Finally, again, we take $\nu_{\text{NO}} = 0$ values for NO-Xe, with the NO values from Ref. 20 and the \tilde{C} state origin from Ref. 18, which is consistent with the spectrum presented in Ref. 21; the \tilde{X} state D_0 value is taken as 121.3 cm^{-1} from Ref. 15. These values yield a D_0 value for \tilde{C} (NO-Xe) of 823 cm^{-1} . The calculated \tilde{C} state D_0 values are generally in very good agreement with experiment, with the least good agreement being for NO-Xe, as expected, since these calculations employed the smallest basis set. Some of this disagreement could be related to the difficulty of establishing the dissociation energy of the \tilde{X} states, which are derived from those of the \tilde{A} state,^{15,50,51} where there are quasibound levels past the dissociation limit, but it is clear from Table I that these complexes exert high demands on the quantum chemistry (level of theory and basis set). The good agreement of the appearance of the simulated spectra with the experimental ones does, however, suggest that the origins of the \tilde{C} state spectra have been observed in all cases: for NO-Xe, it was particularly noted that the origin may not have been observed in the experiment,²¹ but the simulation confirms that it was.

IV. FINAL REMARKS

In the present work, we have calculated PESs for an excited state of NO-RG complexes that has lower-lying states of the same symmetry, notably at non-linear geometries. Despite this, we were able to calculate both components of the $\tilde{C} \ ^2\Pi$ surface ($^2A'$ and $^2A''$) across a range of geometries, sufficient to obtain a good fitted PES. The close agreement of the simulated spectra for NO-Ar (Ref. 1) and NO-Kr (present work) suggests that the surfaces are reliable and various approximations we have made in calculating the spectrum only have small effects. Knowing the source of each spectral component allows insight into the assignment of the spectrum, and indicates that significant stretch/bend mixing occurs, even early on in the spectrum, while slightly higher in energy various Fermi resonance interactions are likely occurring, causing further mixing. The overall appearance of the NO-Ar and NO-Kr simulated spectra is similar to that achieved in earlier work by Mack *et al.*,²¹ which were obtained employing the model of Meyer,²² where the two-photon intensity was included explicitly. As noted previously,¹ we take this to imply that the explicit inclusion of the two-photon intensities is not required for this level of agreement. The advantage of the present work is that it is wholly *ab initio*, while in Ref. 21, the spectrum had to be constructed heuristically from adding fitted sections of spectra for the different intermolecular vibrational contributions. We have also only included contributions from the lowest $J = 1/2$ level, but we note that inclusion of further

end-over-end rotational levels will only serve to broaden the spectrum slightly (and we have accounted for the width in our convolution); attempts to include “hot” vibrational bands for NO-Ne were not conclusive in obtaining better agreement between experiment and our simulation. Contributions from excited K_a levels are generally expected to be small, as the spectra were recorded under very cold conditions: it is noted that it is relatively straightforward to cool NO to rotational temperatures <5 K in such experiments, and the K_a levels in the complexes have similar energy spacings. Additionally, we note again that there may be effects from interactions between the \tilde{C} and \tilde{B} states that could affect the experimental spectra associated with different v_{NO} levels—inclusion of these would clearly be challenging.

We note that the expectation values of the Jacobi angles from Ref. 21 were around 70° for both NO-Ar and NO-Kr which are very close to the equilibrium values obtained herein for NO-Kr and in Ref. 1 for NO-Ar. This is reassuring as the complex should not be too floppy close to the minimum, and so these two values would be expected to agree reasonably well. For NO-Ne, the Jacobi angle employed varied between 60° and 85° in Ref. 20, while in the present work, a value $\sim 72^\circ$ is obtained. The fact that different Jacobi bond angles were required in the simulations in Ref. 20 is interesting, as such sensitivity is not expected, and it could be that the empirical fitting of the spectrum is compensating for other aspects, such as the omission of combination bands, or could be an effect of \tilde{C} and \tilde{B} state interactions.

ACKNOWLEDGMENTS

We are grateful to the EPSRC for funding (Grant No. EP/H004815) and for access to the NSCCS resource at the Rutherford Appleton Laboratories. We also thank the University of Nottingham for access to its High Performance Computer Resource. O.V.E. is grateful to the EPSRC and the University of Nottingham for a Ph.D. studentship. We thank Professor M. H. Alexander for his encouragement and discussions. J.K. is grateful for the financial support from the U.S. National Science Foundation through Grant No. CHE-1213332 to Professor M. H. Alexander.

- ¹O. V. Ershova, J. Klos, J. P. Harris, A. M. Gardner, V. M. Tamé-Reyes, A. Andrejeva, M. H. Alexander, N. A. Besley, and T. G. Wright, *J. Chem. Phys.* **138**, 214313 (2013).
- ²A. T. B. Gilbert, N. A. Besley, and P. M. W. Gill, *J. Phys. Chem. A* **112**, 13164 (2008).
- ³N. A. Besley, A. T. B. Gilbert, and P. M. W. Gill, *J. Chem. Phys.* **130**, 124308 (2009).
- ⁴M. C. Heaven, *Annu. Rev. Phys. Chem.* **43**, 283 (1992).
- ⁵D. Skouteris, D. E. Manolopoulos, W. Bian, H.-J. Werner, L.-H. Lai, and K. Liu, *Science* **286**, 1713 (1999).
- ⁶E. Miescher and K. P. Huber, “Electronic spectrum of the NO molecule,” *International Review of Science, Physical Chemistry Series 2* (Butterworths, London-Boston, 1976), p. 37.
- ⁷R. S. Mulliken, *J. Am. Chem. Soc.* **86**, 3183 (1964).
- ⁸R. S. Mulliken, *J. Am. Chem. Soc.* **88**, 1849 (1966).
- ⁹R. S. Mulliken, *J. Am. Chem. Soc.* **91**, 4615 (1969).
- ¹⁰J. Lozeille, S. D. Gamblin, S. E. Daire, T. G. Wright, and D. M. Smith, *J. Chem. Phys.* **113**, 7224 (2000).
- ¹¹V. L. Ayles, R. J. Plowright, M. J. Watkins, T. G. Wright, J. Klos, M. H. Alexander, P. Pajón-Suarez, J. Rubayo-Soneira, and R. Hernández-Lamonedá, *Chem. Phys. Lett.* **181**, 441 (2007).
- ¹²K. Tsuji, K. Shibuya, and K. Obi, *J. Chem. Phys.* **100**, 5441 (1994).
- ¹³K. Tsuji, K. Shibuya, and K. Obi, *Laser Chem.* **15**, 157 (1995).
- ¹⁴M. J. McQuaid, G. W. Lemire, and R. C. Sausa, *Chem. Phys. Lett.* **227**, 54 (1994).
- ¹⁵S. D. Gamblin, S. E. Daire, J. Lozeille, and T. G. Wright, *Chem. Phys. Lett.* **325**, 232 (2000).
- ¹⁶J. Klos, M. H. Alexander, R. Hernández-Lamonedá, and T. G. Wright, *J. Chem. Phys.* **129**, 244303 (2008).
- ¹⁷J. C. Miller and W.-C. Cheng, *J. Phys. Chem.* **89**, 1647 (1985).
- ¹⁸J. C. Miller, *J. Chem. Phys.* **86**, 3166 (1987).
- ¹⁹A. M. Bush, J. M. Dyke, P. Mack, D. M. Smith, and T. G. Wright, *Chem. Phys.* **223**, 239 (1997).
- ²⁰J. Fleniken, Y. Kim, and H. Meyer, *J. Chem. Phys.* **109**, 8940 (1998).
- ²¹P. Mack, J. M. Dyke, D. M. Smith, T. G. Wright, and H. Meyer, *J. Chem. Phys.* **109**, 4361 (1998).
- ²²H. Meyer, *J. Chem. Phys.* **107**, 7732 (1997).
- ²³Y. Shao, L. Fusti-Molnar, Y. Jung, J. Kussmann, C. Ochsenfeld, S. T. Brown, A. T. B. Gilbert, L. V. Slipchenko, S. V. Levchenko, D. P. O’Neill, R. A. Distasio, Jr., R. C. Lochan, T. Wang, G. J. O. Beran, N. A. Besley, J. M. Herbert, C. Y. Lin, T. Van Voorhis, S. H. Chien, A. Sodt, R. P. Steele, V. A. Rassolov, P. E. Maslen, P. P. Korambath, R. D. Adamson, B. Austin, J. Baker, E. F. C. Byrd, H. Dachsel, R. J. Doerksen, A. Dreuw, B. D. Dunietz, A. D. Dutoi, T. R. Furlani, S. R. Gwaltney, A. Heyden, S. Hirata, C.-P. Hsu, G. Kedziora, R. Z. Khalliulin, P. Klunzinger, A. M. Lee, M. S. Lee, W. Liang, I. Lotan, N. Nair, B. Peters, E. I. Proynov, P. A. Pieniazek, Y. M. Rhee, J. Ritchie, E. Rosta, C. D. Sherrill, A. C. Simmonett, J. E. Subotnik, H. L. Woodcock III, W. Zhang, A. T. Bell, A. K. Chakraborty, D. M. Chipman, F. J. Keil, A. Warshel, W. J. Hehre, H. F. Schaefer III, J. Kong, A. I. Krylov, P. M. W. Gill, and M. Head-Gordon, *Phys. Chem. Chem. Phys.* **8**, 3172 (2006).
- ²⁴O. V. Ershova and N. A. Besley, *Chem. Phys. Lett.* **513**, 179 (2011).
- ²⁵O. V. Ershova and N. A. Besley, *J. Chem. Phys.* **136**, 244313 (2012).
- ²⁶E. A. Briggs and N. A. Besley, *Phys. Chem. Chem. Phys.* **16**, 14455 (2014).
- ²⁷T. H. Dunning, *J. Chem. Phys.* **90**, 1007 (1989).
- ²⁸R. A. Kendall, T. H. Dunning, and R. J. Harrison, *J. Chem. Phys.* **96**, 6796 (1992).
- ²⁹D. E. Woon and T. H. Dunning, *J. Chem. Phys.* **98**, 1358 (1993).
- ³⁰D. E. Woon and T. H. Dunning, *J. Chem. Phys.* **100**, 2975 (1994).
- ³¹K. A. Peterson, D. Figgen, E. Goll, H. Stoll, and M. Dolg, *J. Chem. Phys.* **119**, 11113 (2003).
- ³²K. P. Huber and G. Herzberg, *Molecular Spectra and Molecular Structure. IV. Constants of Diatomic Molecules* (Van Nostrand, New York, 1979).
- ³³A. M. Bush, T. G. Wright, V. Špirko, and M. Juřek, *J. Chem. Phys.* **106**, 4531 (1997).
- ³⁴P. McGuire and D. J. Kouri, *J. Chem. Phys.* **60**, 2488 (1974).
- ³⁵HIBRIDON is a package of programs for the time-independent quantum treatment of inelastic collisions and photodissociation written by M. H. Alexander, D. E. Manolopoulos, H.-J. Werner, B. Follmeg, Q. Ma, and P. J. Dagdigian with contributions by P. F. Vohralik, D. Lemoine, G. Corey, R. Gordon, B. Johnson, T. Orlikowski, A. Berning, A. Degli-Esposti, C. Rist, B. Pouilly, G. van der Sanden, M. Yang, F. de Weerd, S. Gregurick, J. Klos, and F. Lique. See <http://www2.chem.umd.edu/groups/alexander/hybridon/hib43> for more information and/or a copy of the code.
- ³⁶J. Klos, M. H. Alexander, and H. Meyer, “Joint experimental-theoretical investigation of the bound states of the NO(X)-Ne complex,” *J. Phys. Chem. A* (to be published).
- ³⁷B. Wen, H. Meyer, J. Klos, and M. H. Alexander, *J. Phys. Chem. A* **113**, 7366 (2009).
- ³⁸J. Klos, F. J. Aoiz, M. Menéndez, M. Brouard, H. Chadwick, and C. J. Eyles, *J. Chem. Phys.* **137**, 014312 (2012).
- ³⁹M. H. Alexander, *Chem. Phys.* **92**, 337 (1985).
- ⁴⁰J. W. C. Johns, J. Reid, and D. W. Leppard, *J. Mol. Spectrosc.* **65**, 155 (1977).
- ⁴¹M. Alexander, P. Soldán, T. G. Wright, Y. Kim, H. Meyer, P. Dagdigian, and E. P. F. Lee, *J. Chem. Phys.* **114**, 5588 (2001).
- ⁴²I. P. Hamilton and J. C. Light, *J. Chem. Phys.* **84**, 306 (1986).
- ⁴³M. H. Alexander, *J. Chem. Phys.* **111**, 7435 (1999).
- ⁴⁴M. Hippler and J. Pfab, *Mol. Phys.* **94**, 313 (1998).
- ⁴⁵W. M. Fawzy and J. T. Hougen, *J. Mol. Spectrosc.* **137**, 154 (1989).
- ⁴⁶See supplementary material at <http://dx.doi.org/10.1063/1.4905563> for the individual calculated MOM-MP2 energies from which the PESs were constructed; the interaction energy is given in cm^{-1} and the Jacobi coordinates are given in bohr and degrees. Also, appropriate files required for running the calculations with HIBRIDON (Ref. 35) are given—see

the README_Potentials file. Also contained there are the calculated rovibrational energy levels, with separate files for NO-Ne, NO-Kr, and NO-Xe, obtained from the spin-including calculations, as described in the text—see the README_Bound_States file.

⁴⁷E. P. F. Lee, P. Soldán, and T. G. Wright, *J. Phys. Chem. A* **102**, 6858 (1998), and references therein.

⁴⁸M.-L. Dubernet, D. Flower, and J. M. Hutson, *J. Chem. Phys.* **94**, 7602 (1991).

⁴⁹A. Lagerqvist and E. Miescher, *Helv. Phys. Acta* **31**, 221 (1958).

⁵⁰H. L. Holmes and W. D. Lawrance, *J. Chem. Phys.* **135**, 014302 (2011).

⁵¹W. G. Roeterdink, K. E. Streker, C. C. Hayden, M. H. M. Janssen, and D. W. Chandler, *J. Chem. Phys.* **130**, 134305 (2009).